Sea c g f e de ce f . ca ec f ca : . ca d ced ea . age a ca ac c f g a

Somayeh M. A. Mirzaee and Jean-Michel

medium and the incident electric field strength (E) is described as follows:

$$P_i = \varepsilon_0(\chi^{(1)}_{ij}E_j + \chi^{(2)}_{ijk}E_jE_k + \chi^{(3)}_{ijkl}E_jE_kE_l\ldots + \chi^{(5)}_{ijklmn}E_jE_kE_lE_mE_n + \ldots), \quad (1)$$

in which $\chi^{(n)}$ is an n-rank tensor that is the nth-order optical susceptibility and ε_0 is the permittivity of a vacuum. The lowercase Latin alphabet subscripts denote the Cartesian coordinates, which, according to the Einstein notation, are summed up when repeated in a product. For example, consider a polar crystal with nonzero second-order susceptibility $\chi^{(2)}$ being illuminated by a laser beam with polarization along the c axis whose electric field strength is represented as $E(t) = E_0e^{-i\omega t} + c.c.$ Equation (1) gives the generated second-order nonlinear polarization in the absence of dispersion along the c axis in the crystal as $P^{(2)}(t) = 2\varepsilon_0\chi^{(2)}EE^* + (\varepsilon_0\chi^{(2)}E^2e^{-i2\omega t} + c.c.)$. It consists of a static component at zero frequency plus another one oscillating at frequency 2ω. The latter component is the source term for radiation at the second-harmonic frequency. As the second time derivative of the first component vanishes, it does not lead to the generation of electromagnetic radiation in the DC regime; instead, it induces a static electric field across the nonlinear crystal. This is known as optical rectification (OR). As seen in Eq. (1), the DC polarization of the material depends on the square of the incident electric field. Considering the first order in $\chi^{(2)}$, a static charge distribution will be created inside the nonlinear material that will be linearly proportional to the polarization induced by OR. Since the induced charge is a surface charge that remains bound, only capacitive coupling will make it possible to detect the OR signal as a photovoltage inside a material or structure. A capacitor configuration can be used as shown in Fig. 1. The induced voltage across the electrodes can be expressed as $V \propto \rho \propto \chi^{(2)}2|E$

The samples were illuminated with the laser-source-generating polarized light pulses centered at 1550 nm wavelength. The sample was placed at the focal plane of a focusing lens. The photodiode-generated voltage versus the input illumination power is shown in Fig. 3(a). Different samples show slightly different photoresponses; these differences are attributed to the fabrication and annealing conditions as well as to the aging of the samples.

As it is shown, the slope of the experimental data is very close to 3 decades of photovoltage per decade of optical power in a log–log scale, which can be described by Eq. (1). There, it is clear from the time averaging that only the odd orders of polarization can contribute to the absorption process under a monochromatic field. Consequently, a 3PA process is proportional to the fifth-order nonlinear polarization, and the absorbed energy is proportional to the cube of the light intensity. Furthermore, the 3PA photocurrent from Fig. 3(a) can be correlated with the short circuit current J_{SC} delivered by the same samples under 100 mW/cm^2 illumination from a solar simulator. The results are represented in Table 1 of Ref. [17], which shows that J_{SC} follows the same trend as the 3PA short-circuit (J_{3PA}) photocurrent.

Thus, checking the dependency of the output photovoltage versus the pump power can be considered the simplest measurement test for any multiphoton absorption source versus the optical rectification one.

What can we conclude if the dependency of the output photovoltage versus the pump power is not explainable by the bulk absorption spectrum? To explain this situation, our next set of experiments reveals additional evidence about the MPA process and its differences from the OR mechanism.

B. I d ced P age a Dee S a e M . Ab .

Another possibility to study MPA is through the deep trap absorption of the P3HT blend, which is different from the bulk absorption. Various reports confirm the presence of localized states within the band gap [24,25]. Some variations in photodiode fabrication conditions, like the presence of oxygen, can increase the density of available deep traps. Figure 3(b) shows the evolution of the generated photovoltage versus light power for newly fabricated photodiodes. The slope of the curve is very close to 2 decades of photovoltage per decade of optical power in a log–log scale, which shows that the dominant MPA in these cells is two-photon absorption (TPA). The TPA behavior of photodiodes can be explained by the localized states within the band gap at the interfaces [26]. However, to confirm that these observations are due to the actual TPA and not to other possible photogeneration events, we investigate the effects of the polarization state of the incident light on the intensity of the detected signal.

The TPA photoresponse to the polarized light shows an almost constant dependence versus linear polarization and some oscillatory dependence versus circular polarization, as seen in Fig. 3(c). Small variations from the linear fit in Fig. 3(c) for linearly polarized light are just due to the change in Fresnel coefficients at the air–glass interface with a maximum at p-polarized light. It has been identified that the measured TPA photovoltage for the circularly polarized incident light

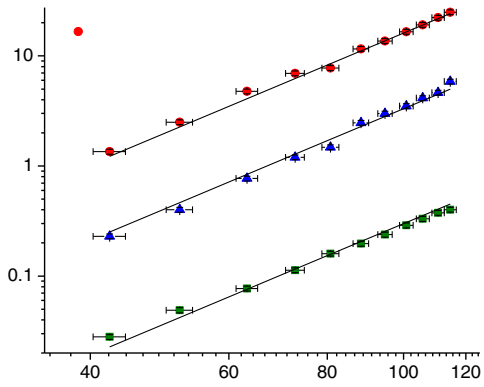

configuration are the photon-drag effect [32,33], current injection [34], drift current [35], and photo-Dember effect [36,37]. However, most of these effects are not relevant to the response of the capacitor structure under study.

D. Induced Photovoltage via Optical Rectification Process in Plasmonic Metal–Semiconductor Interface

In this section, we apply the same methodology as in previous sections to study the OR generated photovoltage via a nanostructured metallic thin film. Despite the large number of reports on metal surface and bulk contributions to SHG [38,39], there are not so many reports on studying the optical rectification process in nanostructured metallic thin films [40], and to our knowledge, no OR voltage could be detected for bare metallic thin films.

In our study, several silver and gold thin films were prepared on ITO substrates in order to optimize the process and parameters for generating a plasmonic nanostructure with significant absorption at 1550 nm [41–44]. The optical absorption spectrum and scanning electron microscope (SEM) image of a 14 nm gold thin film are shown in Figs. 4(a) and 4(b), respectively. The broadened absorption spectrum covering the near-infrared (NIR) region plus the SEM image confirm that the rough thin film consists of randomly placed isolated Au nano-islands with strong interparticle interaction between neighboring particles [45,46].

A capacitor device built from the gold sample in the same configuration represented in Fig. 4(b) was used for photovoltage measurements. The dependency of the output photovoltage

laser), respectively. As is known, in a centrosymmetric material and according to the dipole approximation, the second-order bulk nonlinear susceptibility must vanish [4]. Therefore, the detected SHG signal is due to the broken inversion symmetry at the interface, where the only three nonvanishing independent second-order susceptibility tensor components are $\chi_{zzz}, \chi_{zxx} = \chi_{zyy}$ and $\chi_{xxz} = \chi_{xzx} = \chi_{yyz} = \chi_{yzy}$ [47]. In the illumination configuration shown in Fig. 2 and for an s-polarized incident light, the χ_{zzz} component, which is the largest surface nonzero second-order susceptibility element [39], does not contribute to the SHG emission.

Unlike the SHG signal, which only arises in non-centrosymmetric materials, the THG is allowed in all materials, since the third-order susceptibility $\chi^{(3)}$ is non-vanishing regardless of the symmetry of materials. There are 21 nonzero elements left for the third-order nonlinear susceptibility tensor of an isotropic media, from which only three are independent. The main relation between these nonzero elements is $\chi_{yyyy} = \chi_{xxxx} = \chi_{zzzz} = \chi_{zzyy} + \chi_{zyzy} + \chi_{zyyz}$ [48,49]. So, it is expected to get a larger THG signal when the sample is irradiated by an s-polarized light. Interestingly, owing to the non-phase-matched conditions of the process, the largest contributions to THG will come from the interfaces [50].

Surprisingly, the DC photovoltage polarization plotted in Fig. 6(c) shows a similar behavior to THG emission and not to the SHG one. This indicates the SHG and OR signals have different origins in this sample. The process, which can also explain photovoltage enhancement under s-polarized illumination, is explained below.

The polarization giving rise to the OR signal needs not necessarily be second-order in the pump light's electric field. It has been shown that when suitable combinations of frequencies and static fields are used, higher-order nonlinear polarizations can also lead to rectification [51]. In this situation, the rectification process is via a third-order nonlinear optical process in Eq. (1) called electric-field-induced optical rectification (EFIOR):

$$P_i^{(0)} = \chi_{ijkz}^{(3)}(0; \omega, \omega, DC) E_j^{(\omega)} E_k^{(\omega)} E_z^{DC}, \quad (4)$$

where E_z^{DC} is the DC electric field normal to the surface, proportional to the static depletion field. It has been shown that at the ITO/gold interface, a local depletion forms due to hot-electron injection from gold into the ITO layer [52], which leads to a local rectifying Schottky barrier. Therefore, the features of the DC photovoltage shown in Fig. 6(c) can be explained using the same tensor components as for THG and both are related to the $\chi_{ijkz}^{(3)}$ elements.

We believe that our proposed method of study could reveal the true origin of the detected photovoltage from the metallic nanostructure under intense illumination to be EFIOR but not the normally expected second-order nonlinear OR process, although some contribution from the latter one cannot be ruled out.

4. CONCLUSIONS

Production of electrical DC photovoltage through thin-film illumination has several applications in energy conversion and broadband photodetection. While there has been ongoing research on the nonlinear optical rectification (OR) process as a source of DC photovoltage generation, evidence in the literature and in our own results suggests that there are other nonlinear processes that may contribute to DC photovoltage generation during OR detection in capacitor configuration experiments. Herein, we developed techniques to investigate the true origins of the detected DC photovoltage in an OR detection setup. A clear interpretation of induced photovoltage is an asset to further pursue signal enhancement for potential applications. In summary, the induced photovoltage via multiphoton absorption, work function variations, and optical rectification processes were studied in similarly designed experiments. Our results suggest a baseline to study the origin of the detected photovoltages under an intense illumination through some characteristic tests such as (1) studying the photovoltage scaling with fundamental power, and (2) studying the outcomes of linear and circular polarization variations of the light source on the induced photovoltages.

We finally considered the implications of these tests for a metal nanostructure in a capacitor configuration to address the true origin of the detected OR photovoltage, which proved to be different from the expected one.

Ultimately, we believe that advances in the photovoltage generation via the optical rectification process may give rise to additional unprecedented applications in light detection technologies, rectifying antenna photovoltaics, and sensing applications.

APPENDIX A: ORGANIC PHOTODETECTORS [53]

The glass slides, coated with a patterned indium tin oxide (ITO) layer of 120–160 nm with a sheet resistance of 9–15 Ω/sq, were bought from Lumtec. The ITO slide was cleaned with water, isopropanol, and acetone by sonication in an ultrasonic cleaner for 10 min in each solvent. The slide was dried with a stream of nitrogen. A thin film of zinc oxide (ZnO) was used on top of the ITO electrode as the interface layer to create a more efficient charge transfer path. A solution of 0.75 M zinc acetate dihydrate in 0.75 M monoethanolamine in 2-methoxyethanol was stirred for about 12 h. The solution was then spin-coated on the patterned ITO on a glass slide at 2000 rpm for 40 s to get a layer thickness of about 40 nm. The slide was then baked on a hot plate for 5 mins at 275°C, and then rinsed with deionized water, isopropanol, and acetone. The slide was dried under a jet of nitrogen and the solvent was removed by heating at 200°C for 5 min. This slide was then ready to be spin-coated by the active layer of P3HT: PCBM. A solution of P3HT: PCBM (1:1 wt. ratio) in 1,2-dichlorobenzene was stirred for about 12 h. The solution was then filtered through 0:2 μm PTFE filter to remove any aggregates and stored in a vile. In fact, it is advised to sonicate the solution briefly just before spin-coating the layer. The layer was spin-coated on top of the ZnO layer at 600 rpm for 1 min, to get a layer thickness of about 250 nm. Following spin-coating, the slide was annealed at 110°C for about 10 min. A 120 nm thick silver thin film was deposited by vacuum thermal evaporation at a chamber pressure of $\sim 10^{-6}$ Torr and a deposition rate of 1.5 Å/s as the cathode.

APPENDIX B: ITO-BASED CAPACITOR

The ITO glass was cleaned as outlined above. A gold thin film was deposited by vacuum thermal evaporation at a chamber pressure of about 10^{-6} Torr via a deposition rate of 1 Å/s

37. M. Chen, J. Gu, C. Sun, Y. Zhao, R. Zhang, X. You, Q. Liu, W. Zhang, Y. Su, H. Su, and D. Zhang, "Light-driven overall water splitting enabled by a photo-Dember effect realized on 3D plasmonic structures," ACS Nano 10, 6693–6701 (2016).
38. J. E. Sipe, V. C. Y. So, M. Fukui, and G. I. Stegeman, "Analysis of second harmonic generation at metal surfaces," Phys. Rev. B 21, 4389–4402 (1980).
39. F. X. Wang, F. J. Rodriguez, W. M. Albers, R. Ahorinta, J. E. Sipe, and M. Kauranen, "Surface and bulk contributions to the second-order